High-frequency exciton-polariton clock generator

C. Leblanc,[1] G. Malpuech,[1] and D. D. Solnyshkov [1,2]

[1]*Institut Pascal, University Clermont Auvergne, CNRS, SIGMA Clermont, F-63000 Clermont-Ferrand, France*
[2]*Institut Universitaire de France (IUF), F-75231 Paris, France*

Integrated circuits of photonic components are the goal of applied polaritonics. Here, we propose a compact clock generator based on an exciton-polariton micropillar, providing optical signal with modulation frequency up to 100 GHz. This generator can be used for driving polariton devices. The clock frequency can be controlled by the driving laser frequency. The device also features low power consumption (1 pJ/pulse).

I. INTRODUCTION

Optical computing is an important long-standing goal in the field of photonics [1,2]. Different approaches were used in the field during the past 70 years, including analog optical computing [3,4], combined electro-optical circuits [5], photonic neural networks [6], and digital optical computing [7–9]. Integration of the photonic components raises several key problems linked with miniaturization, such as the protection from the parasite reflections, potentially solved by the recently emerged topological photonics [10,11]. But one of the main problems has been linked with the high powers required for optical switching via the Kerr nonlinearity or other mechanisms used in nonlinear optics [12–14]. One option to solve this issue can be to reduce the size of the nonlinear cavities, such as is done for nanolasers [15]. Another option is to enhance nonlinearities using the strong light-matter coupling [16,17], which allows one to use the significant interactions between the matter part of the eigenmodes [18–20].

Cavity exciton polaritons [17] (polaritons) are a good example of such a promising platform showing an increase by a factor of 10^4 with respect to the ordinary Kerr nonlinearity in standard inorganic semiconductors [20,21] as well as in 2D monolayer materials [22,23] and perovskites [24]. Thanks to these properties, many nonlinear polariton devices have already been proposed and implemented [25–29]. Such devices exhibit low operation powers and fast switching times. They can be assembled into logical circuits capable of functioning at very high operating frequencies. However, in order to be correctly tested and to be ultimately useful, these circuits have to be driven not by an external pulsed (or even *cw*) laser, as it is typically the case in experiments, but by an integrated "clock generator" able to provide the expected operation frequency.

In electronics, the clock generators always contain a nonlinear element (such as an inverter), which is often combined with a resonant element (such as a quartz crystal) for frequency stability. The most well-known example is the Pierce oscillator [30]. In general, the nonlinear circuits used for generating oscillations date back to the beginning of the 20th century [31] and are called multivibrators. They are often based on bistable nonlinear elements exhibiting two possible stationary outputs for a given single input. Biasing the bistable element makes it impossible for it to remain in these stationary states, and thus the element is constantly switching between the two at a well defined rate. It is therefore logical to apply this well-developed approach in photonics.

Bistable elements showing low switching powers have been extensively studied in polaritonic systems [32]. Multistability was shown to appear in these systems because of the spin degree of freedom and because of the spin-anisotropic interactions [21,33,34]. However, these works were focused on the stationary regime. On the other hand, the oscillations of coupled polariton modes with nonlinearities started to be studied at the same time, both under pulsed [35] and cw excitation [36]. Usually, Josephson coupling refers to spatially separated modes, but from the mathematical point of view the same coupling concerns spatially coexisting spin components [35]. Such four-mode system was shown to exhibit high-frequency chaotic oscillations [37]. Later, it was shown that the minimal configuration capable of exhibiting both periodic and chaotic oscillations is actually a pointlike system with two spin projections [38]. In a more recent work, a homogeneous cavity-polariton wire was shown [39] to arrange itself into a network of coupled oscillators displaying self-pulsations or dynamical chaos. However, none of these works focused on the precise purpose of high-frequency clock signal generation, that is, on the generation of a relatively strong propagating output signal with a periodic modulation of intensity with well-controlled frequency, and on the optimization of the parameters of the generator.

In this work, we lay the cornerstone for the future polariton computer. We design and optimize a high-frequency polariton clock generator that could be used in various configurations to drive the optical logical devices. The generator has the simplest possible configuration: a single polariton micropillar with an output channel. Coherent nonlinear oscillations based on the parametric scattering have already been observed in a single polariton pillar [40], which makes the implementation of our proposal quite realistic. Before complete polariton circuits are built, the clock generator can be used for testing the switching performance of various nonlinear elements. The operating frequency of such elements is found of the order

of a few hundreds GHz, close to the THz gap, which makes difficult the use of other types of generators, for example, electro-optical ones.

II. THEORETICAL DESCRIPTION

For relatively low wave vectors, the polariton wave function $\psi(r,t)$ is well described by a nonlinear Schrödinger equation (Gross-Pitaevskii equation) with pump and decay. To simplify the initial theoretical description, we neglect the nonparabolicity of the polariton dispersion and the polarization degree of freedom:

$$i\hbar\frac{\partial\psi}{\partial t} = -\frac{\hbar^2}{2m}\Delta\psi + \alpha|\psi|^2\psi + U\psi - \frac{i\hbar}{2\tau}\psi + P\,e^{-i\omega t},$$

(1)

where $m = 5 \times 10^{-5}m_0$ is the typical polariton mass (m_0 is the free electron mass), $\alpha = 5\ \mu\text{eV}\,\mu\text{m}^2$ is the coefficient of polariton nonlinear interactions [41,42], τ is the polariton lifetime (varying from few ps to few hundred ps), $U(\mathbf{r})$ is the confinement potential obtained by lithography (few tens of meV scale), and $P(\mathbf{r})$ is the pump. Its frequency ω is measured with respect to the energy of a free polariton (approximately 1500 meV in this material system). This is a full 2D model, which we shall use for the numerical simulations of the system. The chosen parameters are typical for GaAs samples.

The system we consider, described by the potential $U(x,y)$, consists of a polariton micropillar of a circular cross section (radius R). A single mode in the presence of a quasiresonant pump and nonlinearity is known to be bistable [32], but it cannot exhibit a complex behavior, such as oscillations. To obtain such behavior, at least two modes are required. This can be obtained either by considering two degenerate modes of coupled pillars [36,43] or two nondegenerate modes of a single pillar, which can be two spatial modes [40] or two spin components [38] with a sufficiently large polarization splitting. We have chosen the configuration with two spatial modes of a single pillar, because it offers a good level of control on the splitting between the two modes, crucial for tuning the output frequency. We note that the presence of the output channels brings an extra contribution in the effective decay rate, which makes the configuration based on the splitting between the two spin projections difficult to use, since it requires the polarization splitting to be much larger than the broadening. The cylindrical pillar is supposed to be pumped exactly in the center with a relatively small pumping spot, optimized for the overlap with the two pumped states.

In order to obtain a qualitative understanding of the behavior of the system, we decompose the global wave function $\psi(x,y,t)$ on the basis of the quantized modes of the micropillar $\psi_n(x,y)$. These modes are solutions of the stationary eigenvalue equation $\hat{H}_0\psi_n = E_n\psi_n$, where $\hat{H}_0$ is the conservative part of Eq. (1) with the potential U restricted to a single pillar (without the output channel). The decomposition is written as $\psi(x,y,t) = \sum_n c_n(t)\psi_n(x,y)e^{-iE_n t/\hbar}$, where the complex coefficients $c_n(t)$ are the amplitudes of the corresponding modes, whose absolute values squared $|c_n(t)|^2$ give the emission intensity. Projecting the nonlinear Schrödinger equation (1) on the eigenstates gives a system of coupled
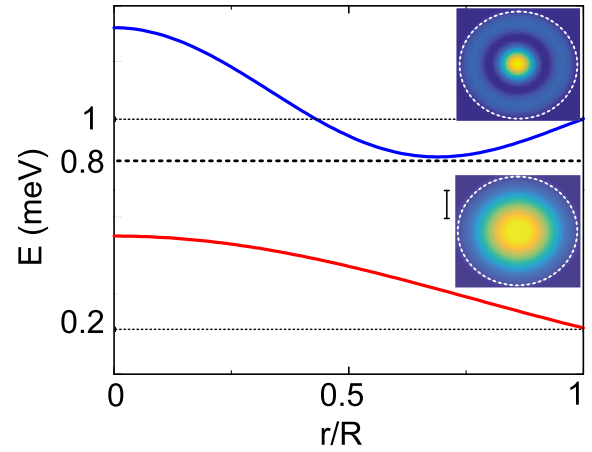

FIG. 1. Energies (dotted lines) and wave functions (solid lines) of the two lowest-energy symmetric modes of a micropillar. A possible position of the laser energy is shown as a dashed line. Inset: spatial images of the two states, with the pillar boundary shown as a white dashed circle.

equations for $c_n(t)$. The coupling appears because of the interacting term $\langle\psi_m|\alpha|\psi|^2|\psi_n\rangle \neq 0$, mixing the eigenstates. We need to take into account only the modes that are supposed to be strongly populated, that is, the modes exhibiting a large overlap integral with the pump. The modes of a cylindrical pillar can be written as $\psi_{n,l} = \chi_{n,|l|}J_{|l|}(kr)e^{il\phi}$, where n, l are the radial and azimuthal quantum numbers, J is the Bessel function of the first kind, $k = \hbar^{-1}\sqrt{2mE_{n,l}}$, χ is a normalization constant, and the energies are determined by the zeros of the Bessel function: $E_{n,l} = \hbar^2 j_{n+1,l}^2/2mR^2$ [$j_{n+1,l}$ is the $(n+1)$st zero of the Bessel function J_l]. Since the pumping is symmetric, all wave functions with nonzero l have a vanishing overlap with the pump. The two states of interest, the closest to the bottom and thus the easiest to obtain and to observe, shall be denoted as $\psi_a = \psi_{0,0}$ and $\psi_b = \psi_{1,0}$ (see Fig. 1). The projection of the nonlinear term $|\psi|^2$ can be simplified by analyzing the expected behavior. Indeed, only the ground state can exhibit a bistable jump and become strongly populated, because $E_a < \hbar\omega$. In such conditions, the contribution of the other mode to the coupling term can be neglected. The coupling term therefore reads

$$\langle\psi_a|\alpha|\psi|^2|\psi_b\rangle = \alpha|c_a|^2\iint\psi_a^*|\psi_a|^2\psi_b\,dr\,d\phi = J|c_a|^2.$$

(2)

The sign of J depends on the relative phase of the modes, which, in turn, depends on their actual frequency position with respect to the laser. The two modes are going to have opposite phases because $E_a < \hbar\omega < E_b$ (approximately π phase difference if the decay is neglected), and thus $J < 0$. This can be understood qualitatively as follows: the admixture of the upper state brings the ground state closer to the Thomas-Fermi limit [44]. Numerical evaluation of the Bessel functions gives $JS \approx 1.3\alpha$. For the nonlinear shift in the energy of each mode, we neglect the contribution of the other mode and of the interference terms, because of the smaller overlap integrals.
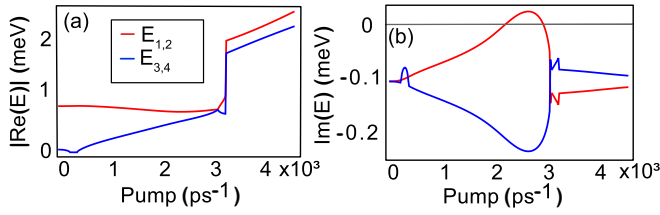
FIG. 2. Real (a) and imaginary (b) parts of the energy of weak perturbations of the stationary solution for a pillar of $R = 4.5$ μm, a polariton lifetime $\tau = 7$ ps, and a laser frequency of $\hbar\omega = 0.9$ meV.

With all these approximations, the coupled mode equations can be written as

$$i\hbar\frac{\partial c_a}{\partial t} = \left(\hbar\omega_a + \alpha_a|c_a|^2 - \frac{i\hbar}{2\tau}\right)c_a + J|c_a|^2 c_b + P_a e^{-i\omega t},$$
$$i\hbar\frac{\partial c_b}{\partial t} = \left(\hbar\omega_b + \alpha_b|c_b|^2 - \frac{i\hbar}{2\tau}\right)c_b + J|c_a|^2 c_a + P_b e^{-i\omega t}.$$
(3)

To simplify the analysis, we then assume $\alpha_a = \alpha_b = \alpha_0$ (the self-interactions in the two modes are approximately the same) and $P_a = P_b = P_0$ (the overlap of the pump with the two modes is almost the same). In order to identify the necessary conditions for the oscillations, we then perform a stability analysis. We begin by writing the system (3) in the stationary limit, where the only frequency in the system is the laser frequency, $\psi_{a,b}(t) = \psi_{a,b}^s e^{-i\omega t}$:

$$\left(\hbar(\omega_{a,b} - \omega) + \alpha_0\left|c_{a,b}^s\right|^2 - \frac{i\hbar}{2\tau}\right)c_{a,b}^s + J\left|c_a^s\right|^2 c_{b,a}^s + P_0 = 0.$$

Following the Bogoliubov–de Gennes approach, we study the weak perturbations of the stationary solution $\psi_{a,b}(t) = e^{-i\omega t}(\psi_{a,b}^s + U_{a,b}e^{-iEt/\hbar} + V_{a,b}^* e^{iE^*t/\hbar})$, which results in a secular equation allowing one to find the eigenenergies E of these excitations. The positive imaginary part $\text{Im} E > 0$ of any eigenvalue means that the corresponding perturbation grows exponentially, and the real part of its energy is a good estimation for the frequency of the self-sustained oscillations $\omega_{osc} \approx \text{Re} E/\hbar$, once a new regime settles down. Figure 2 shows the real and imaginary parts of the energies of weak perturbations as a function of pumping P_0 (parameters given in the caption). We see that there is a range of pumping values (between 2×10^3 and 3×10^3 particles/ps) which correspond to the growth of the perturbations $\text{Im} E > 0$. It is in this range of parameters that our device is expected to operate. Moreover, since the real part of the energy is almost constant in this range, the generator is well protected from the fluctuations of the driving laser intensity.

The approximate frequency of the generated clock oscillations can be found numerically from the solution of the fourth order secular equation, but, in order to have a clear analytical estimate, we need to reduce the system size, keeping only the important terms: the energies of the two modes (taking into account the effect of the bistability) and their coupling. For this estimate, we assume that the frequency of the lower mode jumps to the frequency of the pump, which determines both its energy and its occupancy. The reduced two-coupled modes

Hamiltonian reads

$$\hat{H}_{\text{red}} = \begin{pmatrix} \hbar\omega & J\frac{\hbar\omega - E_a}{\alpha} \\ J\frac{\hbar\omega - E_a}{\alpha} & E_b \end{pmatrix},$$
(4)

which allows one to find the frequency of the oscillations as $\nu = \sqrt{(E_a - \hbar\omega)^2 + 4(E_b - \hbar\omega)^2 J^2/\alpha^2}/2h$ (the factor $1/2$ appears because we analyze the oscillations of intensity). For a pillar of $R = 4.5$ μm with the mode energies of $E_a = 0.2$ meV and $E_b = 1$ meV, and a laser frequency of $\hbar\omega = 0.9$ meV, this expression predicts a frequency of 86 GHz, very close to the value of 91 GHz predicted by the numerical solution of the Bogoliubov–de Gennes equations.

III. RESULTS AND DISCUSSION

In order to check our analytical predictions, we perform two sets of numerical simulations. The first set is based on the full 2D Gross-Pitaevskii equation (1) and the second is based on the two-mode approximation (3). The results of one 2D simulation are shown in Fig. 3 (parameters are given in the caption). Panel (a) shows the spatial distribution of intensity in the system composed of a circular pillar with two output channels. The visible periodic spatial modulation of intensity in the channels is due to the propagating periodically oscillating signal. Figure 3(b) shows the time dependence of the polariton density for a fixed point in a channel, far from the pillar and the boundary of the system. High-contrast stable periodic oscillations are clearly visible. These oscillations set in during the initial transitional period of 1–2 hundreds of ps, and remain stable for at least 40 ns, with no sign of variations with long characteristic time visible over this period. The 2D simulations are too expensive numerically to be carried over much longer times. We have also checked that the oscillations remain stable in the presence of an uncorrelated noise (weak with respect to the pump), simulating the effects of spontaneous polariton scattering.

The corresponding spectral density is shown in panel 3(c). The main frequency is 70 GHz, very close to the simple analytical estimate of 74 GHz provided by the equation (4). This high oscillation frequency is obtained for realistic parameters, as we discuss below. A second harmonic is also
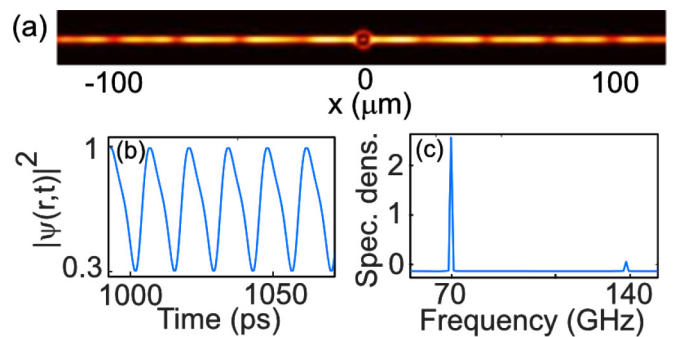

FIG. 3. (a) Spatial polariton density snapshot from a 2D numerical simulation. Propagating density pulses can be observed in the channels. (b) Oscillations of the polariton density for a pillar of $R = 5$ μm, a laser frequency of $\hbar\omega = 0.82$ meV, and a pumping of $p = 2000$ ps^{-1}. (c) Spectral density of $|\psi(r, t)|^2$ showing a resulting frequency of $\nu = 70$ GHz.
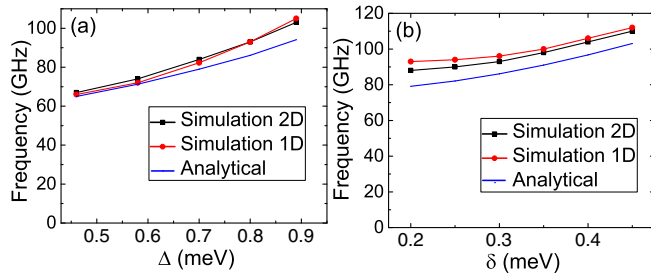

FIG. 4. (a) Frequency as a function of Δ for $\delta = 0.3$ meV constant. (b) Dependence of the frequency with δ for $\Delta = 0.8$ meV constant. The pumping varies between 1500 and 3000 ps^{-1}.

visible in the spectrum; it appears because of the deviation of nonlinear oscillations from perfectly harmonic ones, which is also visible in the time-resolved intensity plot of Fig. 3(b).

Figure 4 presents the dependence of the most practically important parameter—the clock frequency—on the parameters of the system which can be varied experimentally. These parameters include the energy difference between the two modes of the pillar $\Delta = E_b - E_a$ (determined by the size of the pillar) and the laser detuning with respect to the middle frequency $\delta = \hbar\omega - (E_a + E_b)/2$. As an example, for a pillar of $R = 4.5$ μm and a laser frequency of $\hbar\omega = 0.9$ meV, we obtain $\Delta = 0.8$ meV and $\delta = 0.3$ meV. Figure 4(a) shows the increase of the frequency from 70 to above 100 GHz with the increase of mode splitting Δ (for a constant detuning $\delta = 0.3$ meV), meaning the smaller the pillar, the higher the oscillation frequency. The detuning δ of the laser is also an important parameter in order to optimize the output frequency, as shown in Fig. 4(b). Unfortunately, both Δ and δ cannot be increased indefinitely, because the efficiency of the laser pumping decreases with its detuning with respect to the mode. For a mode linewidth of $\gamma \approx 0.1$ meV, the maximal experimentally realistic offset is $\sim 7\gamma \approx 0.7$ meV [42]. It means that the realistic values of δ in Fig. 4(b) are below 0.3 meV. Nevertheless, we provide the results for higher values of δ, which might be accessible for broader pillar resonances.

These two figures confirm that the operation frequency can be tuned in a broad range of values. The most accessible way for tuning the clock generator is via the pumping laser frequency.

We stress that in the 2D simulations the value of the lifetime is different in the pillar (7 ps^{-1}) and in the channels (300 ps^{-1}), which can be easily achieved experimentally. This is important, because it is the decay rate γ which constrains the maximal operation frequency via δ and Δ. Sufficiently high decay rate is required for high-frequency operation. We also note that the generator frequency is relatively stable with respect to the pumping power: it changes only by 10% within the whole range of pumping powers where the oscillations can be observed (for constant Δ and δ). Besides the frequency, another important parameter of the clock generator is the power consumption. The power of the optical pump used to drive the system is of the order of 10 μW. This is approximately 10 times higher than in the best modern electronic clock generators. However, since the operation frequency of the present device is much higher, energy consumption per pulse is of the order of 1 pJ, much better than in electronics.

To conclude, we have studied the possibility of fabrication of a clock generator for integrated polaritonic circuits based on a single polariton micropillar. Such a device demonstrates high generation frequencies of about 100 GHz, required to fully exploit the potential of polariton circuits for ultrafast data treatment. We have shown that the operation frequency can be controlled by the laser detuning (*in situ*) or by changing the pillar radius.

[1] P. Ambs, Adv. Opt. Tech. **2010**, 372652 (2010).

[2] J. Touch, A.-H. Badawy, and V. J. Sorger, Nanophotonics **6**, 503 (2017).

[3] C. Fabre, Nat. Photon. **8**, 883 (2014).

[4] D. R. Solli and B. Jalali, Nat. Photon. **9**, 704 (2015).

[5] Z. Ying, Z. Wang, Z. Zhao, S. Dhar, D. Z. Pan, R. Soref, and R. T. Chen, Opt. Lett. **43**, 983 (2018).

[6] D. Woods and T. J. Naughton, Nat. Phys. **8**, 257 (2012).

[7] A. A. Sawchuk and T. C. Strand, Proc. IEEE **72**, 758 (1984).

[8] J. Touch, Y. Cao, M. Ziyadi, A. Almaiman, A. Mohajerin-Ariaei, and A. E. Willner, Nanophotonics **6**, 507 (2017).

[9] B. S. Wherrett, Digital optical computing, *Nonlinear Optical Materials and Devices for Applications in Information Technology*, edited by A. Miller, K. R. Welford, and B. Daino, NATO ASI Series (Springer, Netherlands, Dordrecht, 1995),Vol. 289, pp. 321–361.

[10] L. Lu, J. D. Joannopoulos, and M. Soljacic, Nat. Photon. **8**, 821 (2014).

[11] T. Ozawa, H. M. Price, A. Amo, N. Goldman, M. Hafezi, L. Lu, M. C. Rechtsman, D. Schuster, J. Simon, O. Zilberberg *et al.*, Rev. Mod. Phys. **91**, 015006 (2019).

[12] N. N. Rozanov, *Spatial Hysteresis and Optical Patterns* (Springer, Berlin, 2002).

[13] R. Reinisch and G. Vitrant, Prog. Quantum Electron. **18**, 1 (1994).

[14] N. I. Zheludev, Sov. Phys. Usp. **32**, 357 (1989).

[15] P. Hamel, S. Haddadi, F. Raineri, P. Monnier, G. Beaudoin, I. Sagnes, A. Levenson, and A. M. Yacomotti, Nat. Photon. **9**, 311 (2015).

[16] J. J. Hopfield, Phys. Rev. **112**, 1555 (1958).

[17] A. Kavokin, J. J. Baumberg, G. Malpuech, and F. P. Laussy, *Microcavities* (Oxford University Press, Oxford, 2011).

[18] C. Ciuti, V. Savona, C. Piermarocchi, A. Quattropani, and P. Schwendimann, Phys. Rev. B **58**, 7926 (1998).

[19] M. Vladimirova, S. Cronenberger, D. Scalbert, K. V. Kavokin, A. Miard, A. Lemaître, J. Bloch, D. Solnyshkov, G. Malpuech, and A. V. Kavokin, Phys. Rev. B **82**, 075301 (2010).

[20] Y. Sun, Y. Yoon, M. Steger, G. Liu, L. N. Pfeiffer, K. West, D. W. Snoke, and K. A. Nelson, Nat. Phys. **13**, 870 (2017).

[21] T. K. Paraiso, M. Wouters, Y. Leger, F. Morier-Genoud, and B. Deveaud-Pledran, Nat. Mater. **9**, 655 (2010).

[22] F. Barachati, A. Fieramosca, S. Hafezian, J. Gu, B. Chakraborty, D. Ballarini, L. Martinu, V. Menon, D. Sanvitto, and S. Kéna-Cohen, Nat. Nanotechnol. **13**, 906 (2018).

[23] R. Emmanuele, M. Sich, O. Kyriienko, V. Shahnazaryan, F. Withers, A. Catanzaro, P. Walker, F. Benimetskiy, M. Skolnick, A. Tartakovskii *et al.*, arXiv:1910.14636.

[24] A. Fieramosca, L. Polimeno, V. Ardizzone, L. De Marco, M. Pugliese, V. Maiorano, M. De Giorgi, L. Dominici, G. Gigli, D. Gerace *et al.*, Sci. Adv. **5**, eaav9967 (2019).

[25] T. Gao, P. S. Eldridge, T. C. H. Liew, S. I. Tsintzos, G. Stavrinidis, G. Deligeorgis, Z. Hatzopoulos, and P. G. Savvidis, Phys. Rev. B **85**, 235102 (2012).

[26] D. Ballarini, M. De Giorgi, E. Cancellieri, R. Houdré, E. Giacobino, R. Cingolani, A. Bramati, G. Gigli, and D. Sanvitto, Nat. Commun. **4**, 1778 (2013).

[27] H. S. Nguyen, D. Vishnevsky, C. Sturm, D. Tanese, D. Solnyshkov, E. Galopin, A. Lemaître, I. Sagnes, A. Amo, G. Malpuech *et al.*, Phys. Rev. Lett. **110**, 236601 (2013).

[28] D. Sanvitto and S. Kéna-Cohen, Nat. Mater. **15**, 1061 (2016).

[29] A. V. Zasedatelev, A. V. Baranikov, D. Urbonas, F. Scafirimuto, U. Scherf, T. Stöferle, R. F. Mahrt, and P. G. Lagoudakis, Nat. Photon. **13**, 378 (2019).

[30] G. W. Pierce, Proc. Am. Acad. Arts Sci. **59**, 81 (1923).

[31] W. H. Eccles and F. W. Jordan, Electrician **83**, 298 (1919).

[32] A. Baas, J.-P. Karr, M. Romanelli, A. Bramati, and E. Giacobino, Phys. Rev. B **70**, 161307(R) (2004).

[33] N. A. Gippius, I. A. Shelykh, D. D. Solnyshkov, S. S. Gavrilov, Y. G. Rubo, A. V. Kavokin, S. G. Tikhodeev, and G. Malpuech, Phys. Rev. Lett. **98**, 236401 (2007).

[34] S. Gavrilov, N. Gippius, S. Tikhodeev, and V. Kulakovskii, JETP **110**, 825 (2010).

[35] I. A. Shelykh, D. D. Solnyshkov, G. Pavlovic, and G. Malpuech, Phys. Rev. B **78**, 041302(R) (2008).

[36] D. Sarchi, I. Carusotto, M. Wouters, and V. Savona, Phys. Rev. B **77**, 125324 (2008).

[37] D. D. Solnyshkov, R. Johne, I. A. Shelykh, and G. Malpuech, Phys. Rev. B **80**, 235303 (2009).

[38] S. S. Gavrilov, Phys. Rev. B **94**, 195310 (2016).

[39] S. S. Gavrilov, Phys. Rev. Lett. **120**, 033901 (2018).

[40] L. Ferrier, S. Pigeon, E. Wertz, M. Bamba, P. Senellart, I. Sagnes, A. Lemaître, C. Ciuti, and J. Bloch, Appl. Phys. Lett. **97**, 031105 (2010).

[41] L. Ferrier, E. Wertz, R. Johne, D. D. Solnyshkov, P. Senellart, I. Sagnes, A. Lemaître, G. Malpuech, and J. Bloch, Phys. Rev. Lett. **106**, 126401 (2011).

[42] H. S. Nguyen, D. Gerace, I. Carusotto, D. Sanvitto, E. Galopin, A. Lemaître, I. Sagnes, J. Bloch, and A. Amo, Phys. Rev. Lett. **114**, 036402 (2015).

[43] M. Abbarchi, A. Amo, V. G. Sala, D. D. Solnyshkov, H. Flayac, L. Ferrier, I. Sagnes, E. Galopin, A. Lemaitre, G. Malpuech *et al.*, Nat. Phys. **9**, 275 (2013).

[44] L. Pitaevskii and S. Stringari, *Bose-Einstein Condensation*, International Series of Monographs on Physics Vol. 116 (Oxford Science Publications, Oxford, 2003).